Techno-Economic Analysis of ZnO Nanoparticles Pretreatments for Biogas Production from Barley Straw

Mohamed A. Hassaan [1,2,*](ID), Antonio Pantaleo [2,*](ID), Francesco Santoro [2](ID), Marwa R. Elkatory [3], Giuseppe De Mastro [2](ID), Amany El Sikaily [1], Safaa Ragab [1] and Ahmed El Nemr [1]

1   Marine Pollution Lab, National Institute of Oceanography and Fisheries, Alexandria 21556, Egypt; dramany_mas@yahoo.com (A.E.S.); safaa_ragab65@yahoo.com (S.R.); ahmedmoustafaelnemr@yahoo.com (A.E.N.)
2   Department of Agriculture and Environmental Sciences, Bari University, 70121 Bari, Italy; francesco.santoro@uniba.it (F.S.); giuseppe.demastro@uniba.it (G.D.M.)
3   City for Scientific Research and Technological Applications, Advanced Technology and New Materials Research Institute, Alexandria 21934, Egypt; marwa_elkatory@yahoo.com
*   Correspondence: Mhss95@mail.com (M.A.H.); antonio.pantaleo@uniba.it (A.P.)

check for updates

Abstract: The aim of this study was to analyze the effect of ZnO nanoparticles (ZnO NPs) on the biogas production from mechanically treated barley straw and to perform a techno-economic analysis based on the costs assessment and on the results of biogas production. The structural changes of mechanically pretreated barley straw were observed using FTIR, XRD, TGA, and SEM. Additionally, both green ZnO NPs prepared from red alga (*Antithamnion plumula*) extract and chemically prepared ZnO NPs were characterized by FTIR, XRD, SEM, and TEM, surface area, and EDX. The results revealed that the biogas production was slightly improved by 14.9 and 13.2% when the barley straw of 0.4 mm was mechanically pretreated with 10 mg/L of both green and chemical ZnO NPs and produced 390.5 mL biogas/g VS and 385 mL biogas/g VS, respectively. On the other hand, the higher concentrations of ZnO NPs equal to 20 mg/L had an inhibitory effect on biogas production and decreased the biogas yield to 173 mL biogas/g VS, which was less than the half of previous values. It was also clear that the mechanically treated barley straw of 0.4 mm size presented a higher biogas yield of about 340 mL/g VS, in comparison to 279 mL biogas/g VS of untreated biomass. The kinetic study showed that the first order, modified Gompertz and logistic function models had the best fit with the experimental data. The results showed that the nanoparticles (NPs) of the mechanically treated barely straw are a suitable source of biomass for biogas production, and its yields are higher than the untreated barley straw. The results of the cost-benefit analysis showed that the average levelized cost of energy (LCOE), adopting the best treatments (0.4 mm + 10 mg/L ZnO), is 0.21 €/kWh, which is not competitive with the other renewable energy systems in the Egyptian energy market.

Keywords: green ZnO nanoparticles; *Antithamnion plumula*; catalysis; barley straw; biogas; kinetic models; cost-benefits analysis; levelized cost of energy

1. Introduction

Biomass is a well-known renewable source to offer energy demand in terms of heat and electricity [1]. The Renewable Energy Directive 2018/2001/EU (RED II) forces the European Union (EU) to increase renewable energy consumption to 32% by 2030 [2]. Anaerobic digestion (AD) is extremely motivating in this framework as it can function in the production of renewable energy in the form of methane (CH_4)-enriched biogas; AD is a reasonably slow microbial centered method that is reliant

on pH, temperature, C:N ratio, and hydraulic retention time [3]. Various kinds of organic materials can be used as substrates for biogas production, such as manure, sewage sludge, and agriculture residues. Among these agricultural residues, straw is a motivating feedstock for the production of biogas [3,4]. For example, barley straw is one of the most worldwide plentiful crop residues. Barley straw is an agricultural residual of barley production with high total solids (TS) content [5,6]. However, the composition and character of lignocellulose, with cellulose fibers intertwined with hemicelluloses and lignin, make it hard to degrade [6]. The biogas revenue from barley straw can be improved by harvesting techniques [7], pretreatment, making the material more reachable to microbial degradation [3,6,8,9]. Feng et al. [5] examined the impact of co-ensiling of cover crops and barley straw on biogas production. The results demonstrate that cover crops are practicable for producing biogas with considerable CH_4 yield (330 mL CH_4/g VS) and has good storability. Mechanical pretreatment typically provides a big surface area in the organic materials, permitting a greater area of contact for the microorganisms that degrade the materials, leading to increased biogas yields, the overall conversion of lignocellulosic biomass into biogas without producing any toxic side streams [10]. The biogas yield of some substrates increases nearly linearly with the increase of the outer surface [11]. Compared with alternative approaches (i.e., sonication, chemical, biological), mechanical pretreatments are typically considered more suitable for industrial applications [12–15]. Balsari et al. [16] studied the effect of mechanically pretreated barley straw (sizes at 5.0, 2.0, and 0.5 cm) on the biogas and methane yield. The pretreated barley straw size 0.5 cm gives the highest yields 784 and 370 (NL kg^{-1} VS) for biogas and methane production, respectively. Nanoparticles (NPs) are currently extensively used in commercialized products. With the exceptional physiochemical characteristics (e.g., optical, magnetic, and electrical features), the usage of NPs is considered perfect in manufacturing trades. Adding additives has become a widely used approach to improve AD performance [17]. Numerous researches have examined the addition of different kinds of NPs to improve the biogas production and enhance AD [16–19]. Mu et al. [20] stated that only chemical ZnO NPs have a reducing impact on methane production. Additionally, the lowering of ZnO NPs dosage (less than 6 mg/g TS) has little or no impact on methane production. Hassaan et al. [21] verified that NPs might enhance the AD process and stimulate the slurry digestion, which improves the biogas generation, but it depends on a certain dosage. The improvement of the biogas production from durum wheat is attained by adding lower concentrations of 5 and 10 µg/mL of ZnO NPs, while the addition of a higher concentration of 20 µg/mL of ZnO NPs has an inhibitory effect.

In this work, the novel designed synthesis procedure based on macroalgae extract for the green synthesis of ZnO NPs with small particle sizes is environmentally friendly, economically affordable, and predominant, preventing using unsafe materials, which are common in conventional chemical methods [22,23]. Four kinetic models—the first-order kinetic, the modified Gompertz, the logistic function, and Cone models—were reported to represent and reproduce the experimental data. However, to the best of our knowledge, the study on the kinetics of biogas production under the influence of NPs stress does not exist. The accuracy of these models was compared by statistical analysis of correlation coefficients (R^2).

As in other biomass usage devoted to energy production [24,25], it is important from an economical point of view to perform a cost-benefit analysis of using mechanical and ZnO NPs treatment for barley straw to produce biogas as the profitability may ultimately determine if farmers and landowners start to utilize this practice. The economic feasibility of biogas production depends on the possible income from the biogas produced versus the total cost of production. These parameters are affected by local and site-specific conditions; for the case of this study, the assumptions made are presented in the results. The cost-benefit analysis performed in this study was based on the whole chain of crop cultivation (land preparation, planting, pesticide, and fertilizer application), harvesting, transport, mechanical (chipping and milling), ZnO NPs treatment, investment, and conversion of the crops at a biogas plant. The costs for these variables are based on prices in Egypt. The levelized cost of energy (LCOE) is an estimation of the economic lifetime energy production and cost [26]. The LCOE is sensitive to minor

alterations in the input variables and expectations. Therefore, the precise values of these input statistics are crucial for consistent results. Furthermore, the sensitivity of the LCOE to different input data must also be estimated. This work aimed to study the impact of green ZnO NPs synthesized from the extract of red algae *Antithamnion plumula* (*A. plumula*) on the mechanically pretreated barley straw with particles size 0.4 mm and untreated (raw) barley straw 4 mm. Based on the literature survey, *A. plumula* alga extract was employed for the first time as a natural nano-factory for ZnO NPs biosynthesis. The content of innovation of this research was to perform an assessment of cost-benefit analysis and LCOE for using nanotechnology in biogas production. According to the knowledge of the author, this was the first work that describes in detail the effect of a combination of mechanical and ZnO NPs treatment based on various cost calculation approaches, such as cost-benefit analysis and LCOE. Moreover, this paper delivered new insights for NPs technologies and its availability of usage on a large scale.

2. Materials and Methods

Figure 1 shows a flow chart of the experimental examinations with the steps of the procedures proposed. Zinc acetate dihydrate and NaOH were obtained from Aldrich Chemicals, Milwaukee, WI, USA.
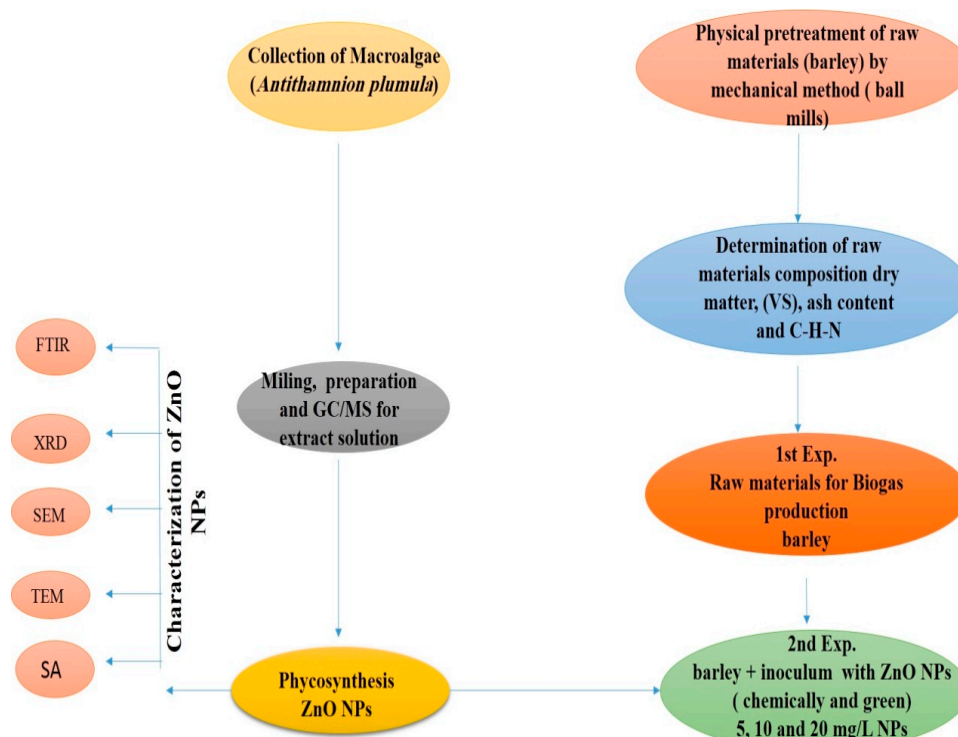

Figure 1. Flow chart of the experimental procedures.

2.1. Inoculum and Substrates Preparation

Barely straw was used as a substrate for this work. An inoculum was obtained from a mesophilic biogas plant in Puglia, Italy. Red algae (*A. plumula*) for ZnO NPs synthesis was collected from the coast of Baltic Sea, Kiel City, Germany (54°453789″ N, 10°197037″ E) in the spring of 2018. The barley cultivation (*Hordeum vulgare* L.) was done at the experimental farm in Puglia, Italy, and was harvested in the spring of 2018. Standard methods [27] were applied for the determination of total solids (TS), volatile solids (VS), and ash content. The C, H, and N measurement was done by the elemental analyzer (LECO Model CHN 628).

2.2. Biogas Experiment

All experiments were implemented with 1 g TS of barley straw (dry weight) and 20 g of inoculum (wet weight) with a concentration of 8.40% TS, followed by mixing for 20 min for homogenization. The inoculum/substrate ratio was set based on the previous works [18,21]. The mechanically pretreated barley straw was dried, milled, and separated to attain a particle size of 0.4 mm using Fritsch, Pulverisette 2, and Filtra vibracion S.L. Other raw samples of barley straw were only dried and cut into small pieces of about 4 mm to fit the digesters. Laboratory tests were implemented in equivalent cylindrical syringes digesters [28–31]. The syringes are reversed straight forward into the lid of the reactor [21,31]. The gas was sampled with a plastic syringe, which was fitted with a 3-way valve and reinjected into the waste. The liquid part of each digester was heated by incubation and monitored with a thermometer situated at the mid-depth and adjusted to 37 ± 1 °C.

Chemical and green ZnO NPs were synthesized from *A. plumula* extract used to study their effects on biogas production from raw and mechanically pretreated barley straw. A stock solution of ZnO NPs at a concentration of 1 g/L was prepared by dispersing nanopowder into MiliQ water (conductivity of 18.2 MU/cm at 25 °C). The stock was then sonicated for 30 min to break aggregates and disperse NPs into the solution. The NPs dispersion was kept in the dark condition in order to prevent the photocatalytic reaction. The stock dispersion of ZnO NPs was stored at 4 °C and used within 24 h of preparation. Then, the prepared ZnO NPs solution was diluted to 5, 10, and 20 mg/L for shock loading in the present study. All the experiments were done in duplicates. The significant difference among the experiments was calculated using the T-test in Microsoft Excel.

2.3. Preparation of Extract from A. plumula

Ten grams of *A. plumula* were washed with sterile double distilled deionized water (SDDW), dried at air temperature (28 °C), and powdered with mortar; then, the powder was added to the Erlenmeyer containing 1000 mL of SDDW. The final mixture was refluxed (70–80 °C) for 3 h, and the mixture was cooled at room temperature (Figure 2). The mixture was centrifuged at 5000 rpm for 5 min, and the small portion of the extract was subjected to GC-MS analysis of the ethanol extract [32].
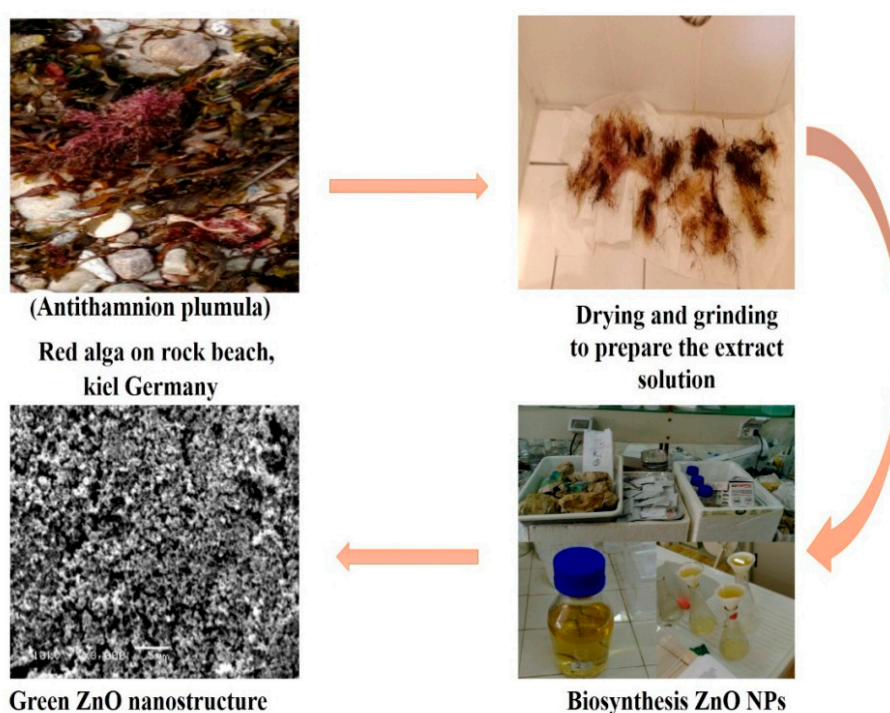

Figure 2. Phycosynthesis route of ZnO nanoparticles (NPs) from *A. plumula* extracts.

2.4. Synthesis of ZnO Nanoparticles (ZnO NPs)

The 10 mL of *A. plumula* extract was mixed with 90 mL of 0.1 M of zinc acetate dihydrate solution drop-wise under continuous agitation at ambient temperature for 4–5 h. After that, 50 mL of 2.0 M NaOH solution was added drop-wise into the above mixture, and the stirring was allowed for 2 h. The resulting white precipitate was filtered and washed repeatedly with distilled water and ethanol to remove the impurities. Finally, the white powder obtained was dried at 60 °C in an oven for 24 h [21,32]. Then, the dried powder was calcinated at 550 °C for 2 h to obtain a pure pale white powder of ZnO NPs (Figure 2), which was carefully collected and used for further investigation. For the chemical synthesis, the same procedures were followed without adding an aqueous extract of the plant [18,21,33].

2.5. Characterization and Measurement

The samples of both ZnO NPs and barley straw (*Hordeum vulgare* L.) before and after mechanical pretreatment were characterized by the following techniques: Fourier transform infrared (FTIR) spectroscopy (platinum ATR) model V-100 VERTEX70, Germany, in the wavenumber range (400–4000 cm^{-1}), X-ray diffractograms (XRD) using a Bruker Meas Srv (D2-208219)/D2-2082019 diffractometer that operates at 30 kV, 10 mA with Cu tube (λ = 1.54 Å), with a range from 0 to 100°. The crystallite sizes were calculated for ZnO NPs using the Scherrer formula. The surface structure was also investigated by Joel 6360LA scan electron microscope (SEM) for both ZnO NPs and barley straw. Thermogravimetric analysis (TGA) of the impregnated sample was carried out by TERIOS Universal V4.5A TA Instruments (New Castle, DE, USA) for barley straw before and after mechanical pretreatment. The prepared nanostructure ZnO (chemically and green) was characterized individually by transmission electron microscope (TEM) (JEOL, Model JSM 6360LA, Tokyo, Japan). The mean pore diameter and specific surface area (BET (Brunauer–Emmett–Teller)) were measured on BELSORP (Mini II, BEL Japan, Inc., Osaka, Japan).

2.6. Kinetics Study and Statistical Analysis

Four kinetic models, i.e., the first-order kinetic model Equation (1), the modified Gompertz model Equation (2), the logistic function model Equation (3), and Cone model Equation (4), were selected to fit the cumulative biogas production obtained from the experimental data [33]. The most suitable kinetic model should be selected not only to predict the efficiency of particular reactors but also to correctly analyze the metabolic pathways [34–36].

All four kinetic models were used in this study to determine the cumulative biogas production potential, hydrolysis kinetics, lag phase duration, and maximum biogas production.

$$M = Pb \times \left(1 - e^{(-kt)}\right) \tag{1}$$

$$M = Pb \times \exp\left\{-\exp\left[\frac{Rm.e}{Pb}(\lambda - t) + 1\right]\right\} \tag{2}$$

$$M = \frac{Pb}{\frac{1+\exp\{4.Rm.(\lambda - t)\}}{pb} + 2} \tag{3}$$

$$M = Pb / \left[1 + (kt)^{-n}\right] \tag{4}$$

where M is the biogas yield (L/g VS added) with respect to time t (days), Pb is the maximum biogas potential of the substrate (L/g VS added), k is the hydrolysis rate constant (1/day), t is the time (day), Rm is the maximum biogas production rate (L/g VS added), λ is the lag phase time (days), e is Euler's function equal to 2.7183. The coefficient of determination (R^2) and root mean square error (RMSE) were calculated for all models to compare the accuracy of the studied models, which was determined using SPSS 15, Origin 2020b, and Excel 2010 software. RMSE, given by Equation (5), was taken as the

standard deviation between the measured and predicted values with a lower RMSE, indicating a well fit [37].

$$\text{RMSE} = \sqrt{\sum_{i=1}^{n} \left(\frac{\text{PVi} - \text{MVi})^2}{n}\right)} \tag{5}$$

where PVi is the predicted value, MVi is the measured value of the biogas volume, and *n* is the number of the measurements.

2.7. Cost Analysis and Economic Indices

The economic feasibility of biogas production depends on the possible income from the produced biogas versus the total cost of production. Both investment and operational costs, including biomass supply, are affected by several site-specific conditions. The cost-benefit analysis performed in this study was based on the whole chain of crop cultivation (preparation of land, planting, pesticide, and fertilizer), harvesting, transport, and conversion of the crops at a biogas plant. The costs for these variables are based on prices in Egypt, where the electricity price is 0.064 €/kWh, the total cultivated area for barley crop is 101,172 ha, with an average yield of 2.96 t DW/ha (personal communications with Egyptian agriculture ministry). Biogas contains roughly 50–70 percent methane, 30–40 percent carbon dioxide, and trace amounts of other gases. In this work, we used 60% for methane production as the proposed percentage to calculate the cost benefits analysis [38]. Moreover, in this work, we used a 40% efficiency of conversion from the literature [39]. Scheme 1 shows the different parameters considered for the cost-benefit analysis.

The LCOE technique has a slighter emphasis as it assesses the producing energy costs from a sole technology. In this technique, elements and resources of the energy system conversion are encompassed, thereby excluding storage, exchange, and final demand effects. This technique usually estimates costs as €/KWh or a dissimilar unit that characterizes the cost of energy generation. The LCOE costs are calculated according to these inputs present in the following Equation (6):

$$\text{LCOE} = \Sigma_t \left[(I_t + M_t + F_t)/(1 + r)^t\right]/\Sigma_t \left[(E_t/(1 + r)^t\right] \tag{6}$$

- The initial cost of investment expenditures in year t (I)
- Maintenance and operations expenditures in year t (M) = 10% of the initial investment cost [38,39]
- Fuel expenditures (if applicable) in year t (F)
- The sum of all electricity generated in year t (E)
- The discount rate of the project (r)
- The life of the system (n)

Calculating the LCOE is linked to the conception of assessing a project's net present value (NPV). NPV is the value of all future cash flows over the entire life of an investment discounted to the present. The formula for the net present value is (Equation (7)):

$$\text{NPV} = \Sigma_i \text{ (Cash flows)}/(1 + r)i - \text{Initial Investment} \tag{7}$$

Cash flows = cash flows in the time period, r = discount rate, and i = time period.

The calculations for cost-benefit analysis and LCOE were made only for green ZnO NPs due to their higher biogas yield than chemical ZnO NPs. The investment costs used to calculate LCOE and NPV are shown in Table 1.
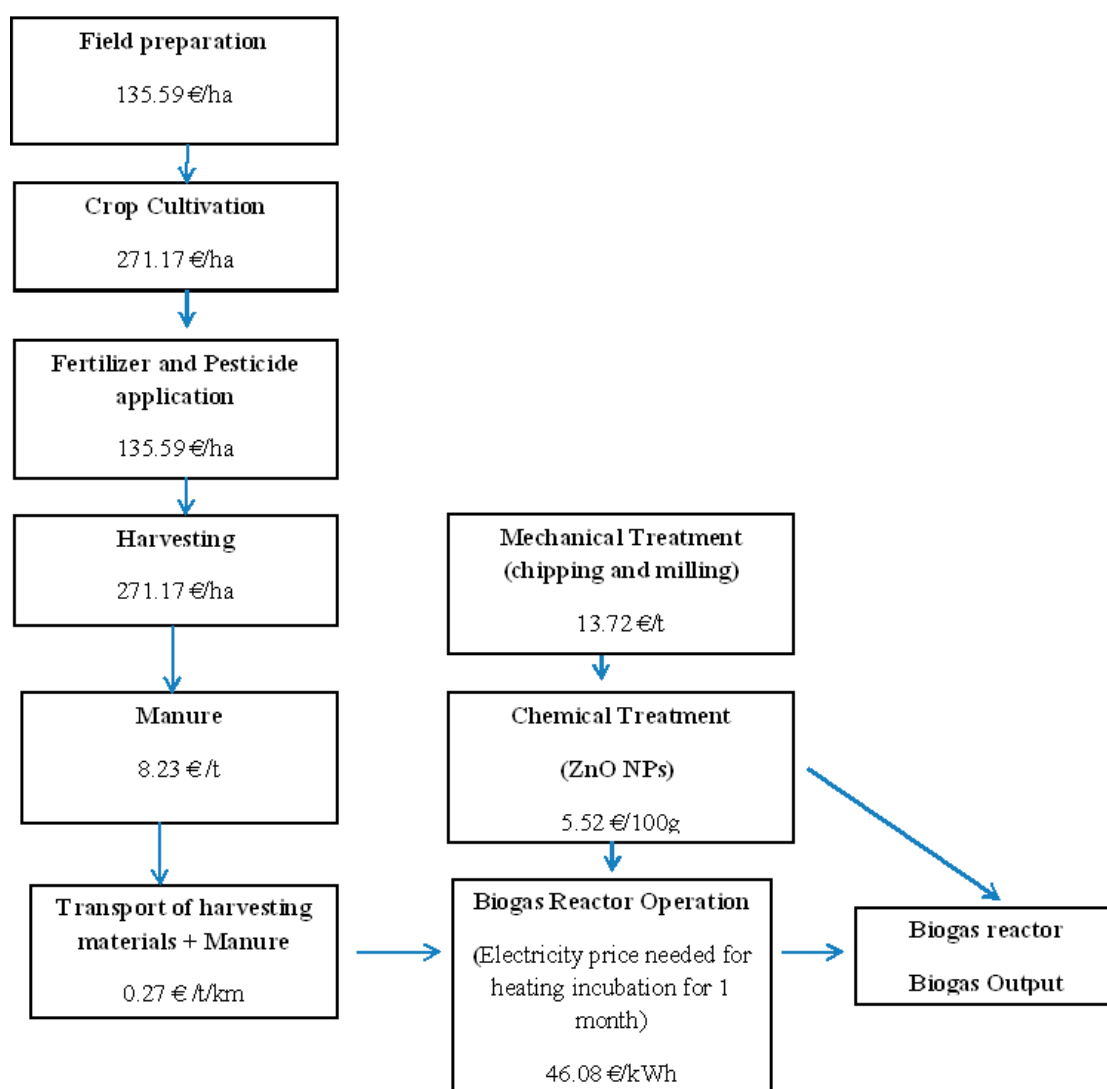
Scheme 1. The different steps in the cultivation and biogas conversion of barley straw, taken into account for the energy balance and cost-benefit analysis.

Table 1. Investment costs for mechanical and chemical treatment of barley straw to calculate LCOE and NPV.

Parameters	Cost
Initial Investment Cost (€)	1000
Annual Operations and Maintenance (O&M) Costs (€)	100
O&M Growth Rate (%)	2%
Annual Fuel Costs (€)	-
Project Lifespan (years)	10
Discount Rate (%)	8%

3. Results and Discussion

3.1. GC-MS Analysis

A broad range of compounds, such as phenols, alcohol, esters, and ethers, can be observed in the GC-MS chromatogram. The GC-MS analysis of ethanol extract of *A.*

plumula shows 11 chemical compounds in Figure 3. Among these compounds, 7.11 min is dodecamethylcyclohexasiloxane, 7.92 min is 5-octadecenal, 9.39 min is 2,4-bis (1,1-dimethylethyl) phenol, 10.26 min is 3-hydroxyspirost-8-en-11-one, 13.41 min is estriol 16-glucuronide, and 14.82 min is 9-desoxy-9x-chloroingol 3,7,8,12-tetraacetate. An assumption of how bioreduction is promoted by these bioactive molecules is as follows: at the initial stage, the metal ions undergo the activation phase, where the growth rate of particles is usually slow as the metal ions are reduced from their salt precursors by the action of plant biomolecule metabolites with reduction capabilities, as shown in Scheme 2. In this work, the reduction of metal ions occurs as a result of biomolecules (2,4-bis(1,1-dimethylethyl)phenol) present in *A. plumula*.
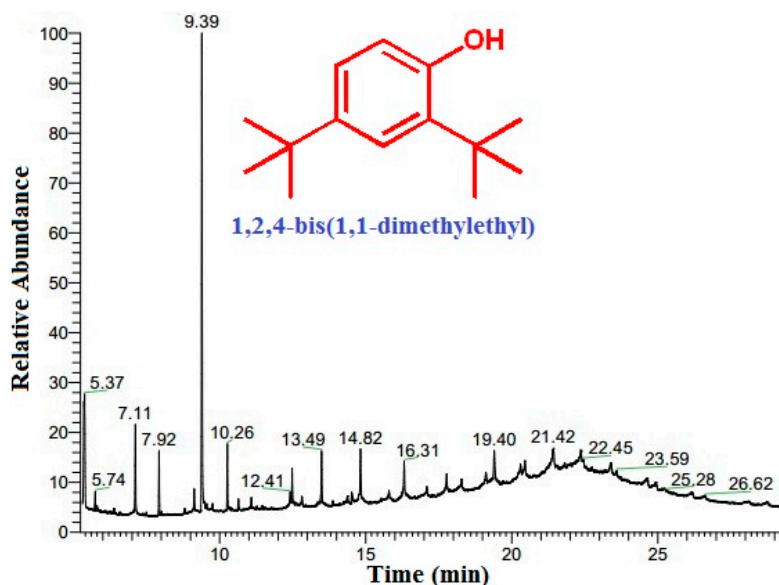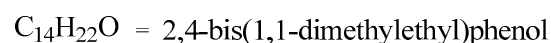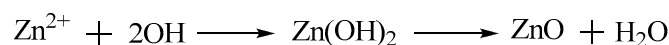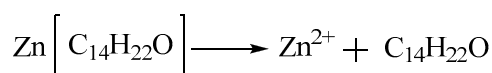

Figure 3. GC-MS chromatogram of *A. plumula* extract.

$$Zn(CH_3COO)_2 \cdot 2H_2O + C_{14}H_{22}O \longrightarrow Zn\left[C_{14}H_{22}O\right] + 2CH_3COO^-$$

$$Zn\left[C_{14}H_{22}O\right] \longrightarrow Zn^{2+} + C_{14}H_{22}O$$

$$NaOH \longrightarrow NaH^+ + OH^-$$

$$Zn^{2+} + 2OH \longrightarrow Zn(OH)_2 \longrightarrow ZnO + H_2O$$

$$C_{14}H_{22}O = 2,4\text{-bis}(1,1\text{-dimethylethyl})\text{phenol}$$
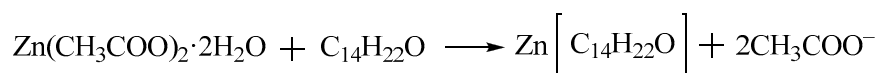
Scheme 2. Mechanism of green synthesis of ZnO NPs.

3.2. Characterization for Barley Straw

3.2.1. Fourier Transform Infrared Spectra (FTIR)

The FTIR shows the overlapping spectra of raw and mechanically pretreated barley straw in Figure 4. The decrease in intensity spectrum of pretreated barley in comparison with raw barley straw in the bands at 1060–1645 cm^{-1} and the broadband at 3000–3820 cm^{-1} suggests the occurrence of deformation in the chemical structure of pretreated barley straw as a result of applying mechanical degradation of lignocellulose [40].
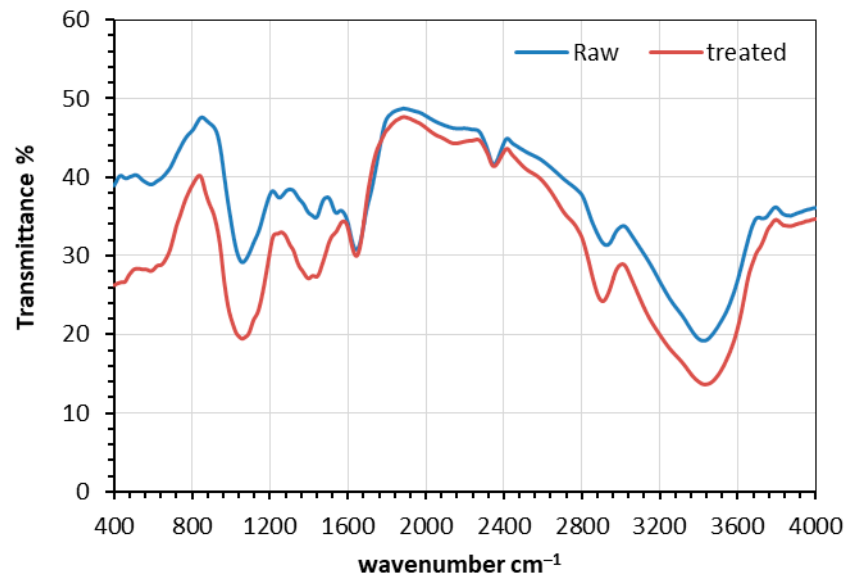
Figure 4. FTIR spectrum of raw and mechanically pretreated barley straw.

3.2.2. X-ray Diffractometry (XRD)

X-ray diffraction analysis is carried out to evaluate the crystallinity degree of the raw and pretreated barley straw, as shown in Figure 5. The crystallography exhibits that the peak intensity of the raw barley sample is at 15.5 and shifts to 22.4 after mechanical pretreatment. A small peak appears post-pretreatment, observed at 15.5, and this corresponds to crystalline cellulose II. The composition of the biomass is highly influenced by crystallinity. The raw material has the lowest relative crystallinity as it has a higher amorphous content of hemicellulose and lignin, and the barley with a high content of lignin and hemicellulose is the barley that presents lower crystallinity, and it could be evidenced that the crystallinity of the pretreated barley increases when treated mechanically [41].
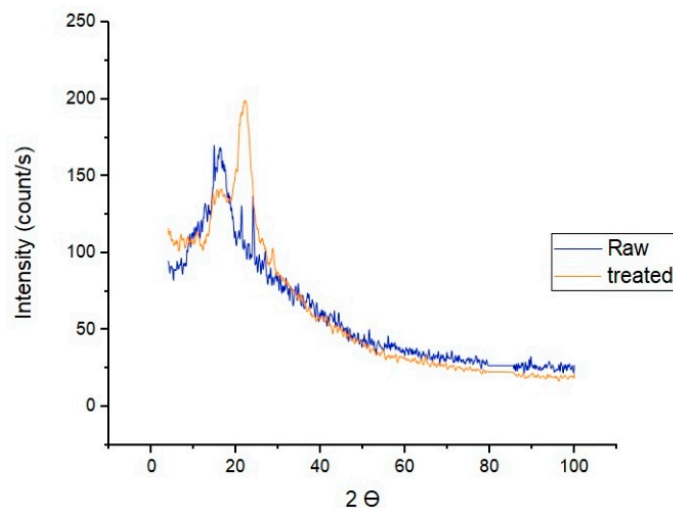

Figure 5. X-ray diffractograms of raw and mechanically pretreated barley.

3.2.3. Scanning Electron Microscopy (SEM)

The SEM images presented in Figure 6 reveal a significant difference between the raw and mechanically treated barley. The results suggest that the raw barley is a sheet structure consisting of fibers connected to each other by a wide pinhole, whereas the pretreated barley straw is broken with tiny pores, and its cell wall has become quite vulnerable due to small particle size to promote the exposure of the cell wall to AD and enhancing biogas production [42].
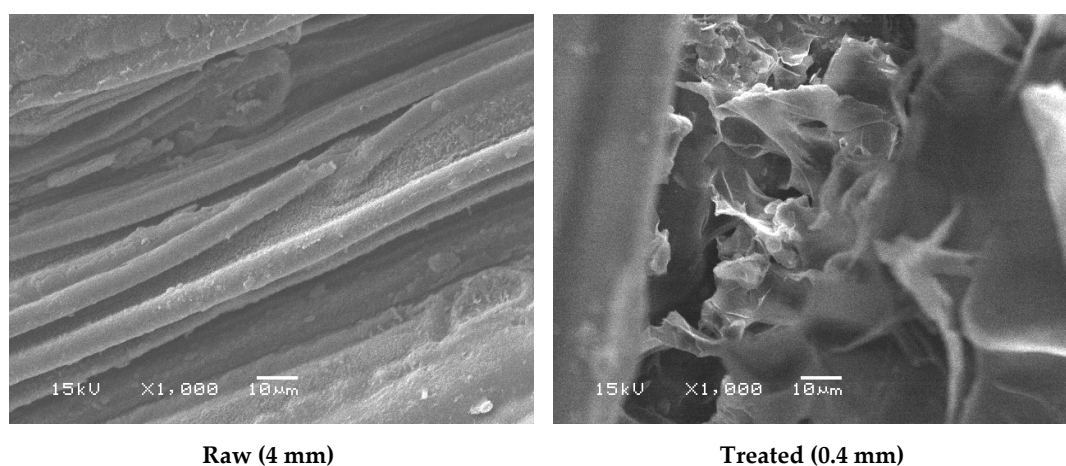
Raw (4 mm)   **Treated (0.4 mm)**

Figure 6. SEM of raw and mechanically pretreated barley.

3.2.4. Thermogravimetric Analysis (TGA)

The biomass thermal stability is examined by means of TGA, the extensively approved method to define the biomass thermal degradation [43,44]. One reflects the evaporation of extractives' desorption of moisture at 100–200 °C, while the others stand for degradation of cellulose and lignin at 300–350 and 300–500 °C, respectively, as shown in Figure 7.
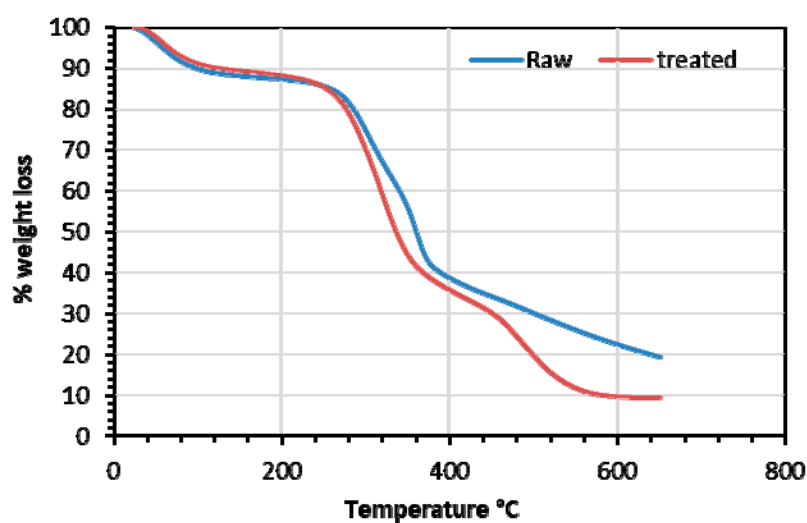

Figure 7. TGA (thermogravimetric analysis) thermographs of raw and mechanically pretreated barley.

3.3. ZnO NPs Characterization

3.3.1. Fourier Transform Infrared Spectra (FTIR)

The FTIR spectra are verified in a frequency range of 400–4000 cm^{-1} to detect the structure of both chemically and green prepared ZnO NPs, as shown in Figure 8. The peak at 557.44 cm^{-1} in Figure 8 corresponds to ZnO, confirming the formation of ZnO NPs [45]. The peaks at 887.21, 1408.08, and 1627.9 cm^{-1} correspond to C–H, C–C, H–O–H, respectively, and are related to an organic compound. The broad peak around 3452.05 cm^{-1} is corresponding to the OH, which represents the presence of water molecules on the surface of ZnO NPs [46–51].
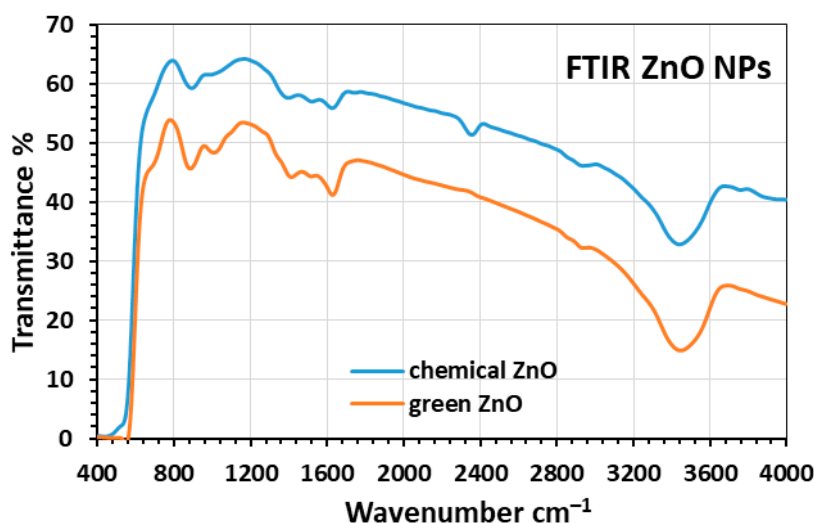
Figure 8. The FTIR spectrum of chemical and green synthesized ZnO NPs.

3.3.2. X-ray Diffractograms

The XRD diffraction pattern of chemically and green synthesized ZnO NPs has been shown in Figure 9. The peaks 2Θare indexed as 31.94 (100), 34.54 (002), 37.08 (101), 47.74 (102), 56.78 (110), 63.02 (103), 66.58 (200), 69.14 (201), 69.36 (201), and 77.28 (202). The obtained peaks demonstrate that the powder is highly crystalline, and all peaks agree with the hexagonal structure that agrees, as stated in the literature [33,45,52,53]. Great purity and crystallinity of the ZnO NPs are shown by the presence of a strong, sharp peak, and the nonappearance of peaks from other zinc oxide and impurity phases. The Scherrer formula is used to calculate the particle sizes and is found to be in the range of 2.7–3.7 and 2.5–3.5 nm, for the chemical and green synthesized ZnO NPs, respectively. The crystallite sizes of the ZnO NPs in Table 2 are estimated by the full width at half maximum (FWHM) of the 101 anatase peak by the Debye–Sherrer Equation (8) [54,55].

$$C_s = 0.89\lambda/\beta cos\theta \qquad (8)$$

where C_s, λ, θ, and β indicate the crystallite size, the X-ray wavelength (1.5406 Å), the Braggs' XRD diffraction angle, and the FWHM in radians, respectively.
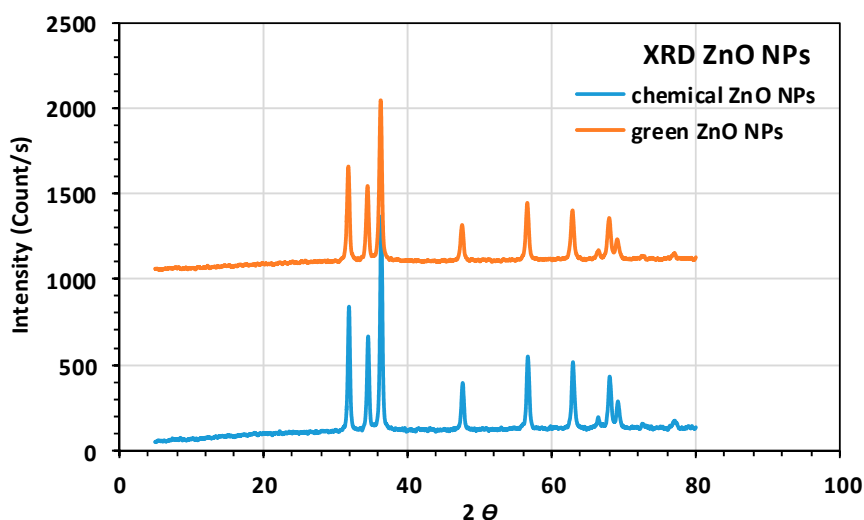

Figure 9. X-ray diffractograms of chemical and green synthesized ZnO NPs.

Table 2. The calculated crystal size of green and chemically synthesized ZnO NPs.

Position	Crystal Size (nm) Chemical ZnO NPs	Crystal Size (nm) Green ZnO NPs
31.94°	3.5	3.3
34.54°	3.7	3.5
37.08°	3.4	3.2
47.76°	3.2	3.0
56.78°	3.1	2.9
63.02°	2.7	2.5
66.58°	3.3	3.1
69.14°	2.6	2.4
69.36°	2.7	2.6
77.04°	3.4	3.2

3.3.3. SEM Microscopy and EDX

Figure 10 shows the morphologies of ZnO NPs structures with spherical morphology grains like and smooth, but clustered grains are composed of many tiny crystallites and clearly illustrate particle loose aggregation. The aggregation of particles (or the creation of larger particles) would have resulted from the large specific surface area of ZnO NPs and the high surface energy, and the synthesized ZnO NPs have a diameter of approximately 5 nm. The energy-dispersive X-ray spectroscopy (EDX) shows the presence of el ts Zn and O in the synthesized ZnO sample. Table 3 indicates the elementary composition together with their weight percentage of chemically and green synthesized ZnO samples, where the contents of Zn on the chemical and green surfaces are 85.01 and 89.4 mass %, respectively, which specifies the greater purity of the green ZnO NPs.

(**Chemical ZnO NPs**)　　　　　　　　　　　　　　　(**Green ZnO NPs**)
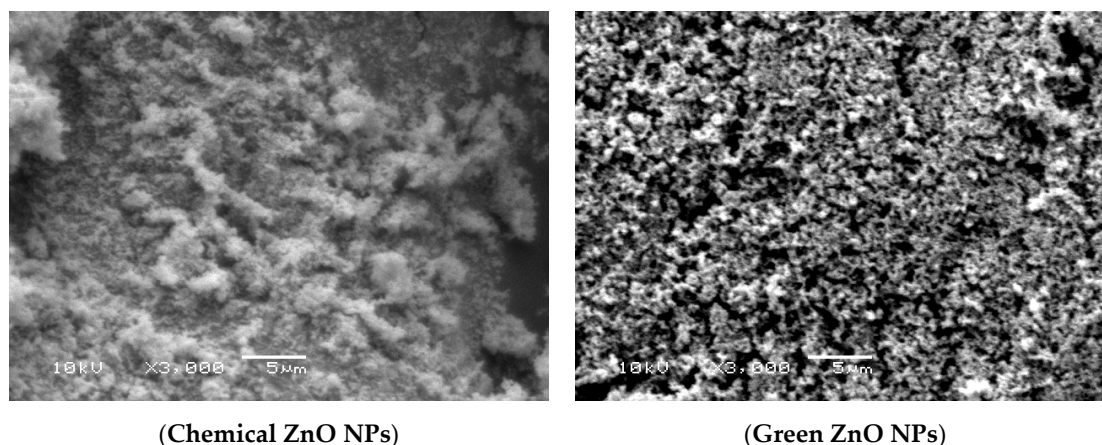
Figure 10. SEM micrograph of chemical and green synthesized ZnO NPs.

Table 3. EDX spectra of chemical and green synthesized ZnO NPs to determine the elemental contents of typical points on the surface.

Elements	Chemical	Green
Zn	85.01	89.4
O	5.72	5.18
Na	9.27	5.42
Total	100%	100%

3.3.4. Transmission Electron Microscope (TEM)

TEM photograph for morphology and distribution of NPs is giving information about the inner core and also gives a more precise finding of particle sizes, as shown in Figure 11. It is evident that the spread nanospheres mixed with little nanorods and incomplete growth of nanorods are formed for both chemically and green synthesized ZnO NPs. The particle size, on average, ranges between 6 and 55 nm.
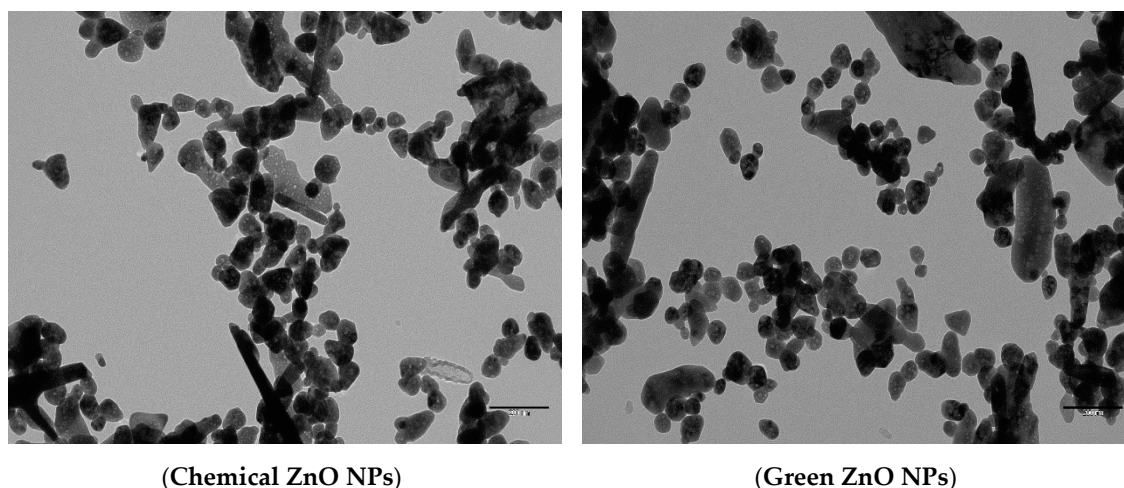

(**Chemical ZnO NPs**)   (**Green ZnO NPs**)

Figure 11. TEM photograph of chemical and green synthesized ZnO NPs.

3.3.5. BET Analysis Surface Area

Table 4 demonstrates using the Brunauer–Emmett–Teller (BET) surface area, and the porous nature of the ZnO NPs is studied. The surface area of ZnO NPs is ranged from 24.33 to 46.47 m^2/g, and the pore volume is ranged from 0.06310 to 0.1479 cm^3/g for both chemical and green synthesized ZnO NPs at the temperature of 550 °C. The average pores diameter is less than 50 nm, which is consistent with the mesoporous material characteristics.

Table 4. BET analysis surface area and the porosity of chemical and green synthesized ZnO NPs.

Sample	BET Surface Area (m^2/g)	Mean Pore Diameter (nm)	Total Pore Volume (cm^3/g)
Chemical ZnO NPs	24.33	10.370	0.0631
Green ZnO NPs	46.47	12.728	0.1479

3.4. Chemical Compositions of Barley Straw

The TS content of the studied barley straw is about 52%, as shown in Table 5. The operated barley straw has no S content. On the other hand, the determination of C and N content is detected by using an elemental analyzer, and the measurement method is carried out following [56]. The C:N ratio is about 33%, as presented in Table 5. Most of the literature works recommend an operating C:N ratio between 20 and 30, with the optimum ratio of 25 for anaerobic bacterial growth in an AD system [57]. The AD of the substrate at an improper C:N ratio will release high total ammonia nitrogen and/or volatile fatty acids (VFA) accumulation in the digester [5]. However, for better methanogenic performance, the optimum C/N ratio is 16–19% when considering hardly degradable complexes like lignin [58–60].

Table 5. The chemical compositions of barley straw.

Component	Barley Straw	Inoculum
TS%	51.9	8.40
Ash%	5.05	28.30
VS%	94.05	71.70
N	1.56	4.30
C	51.15	49.90
H	6.42	5.50
C:N	33.04	9.07

3.5. Effect of Both Mechanical Pretreatment and ZnO NPs on Biogas Production

The biogas production yield is gathered throughout a period of 30 days and charted in Figure 12. The higher biogas production outcomes during the 1st week also agree with the previous literature works [17,61], followed by inactivity, which is probably due to the methanogens undergoing a metamorphic growth process [62].
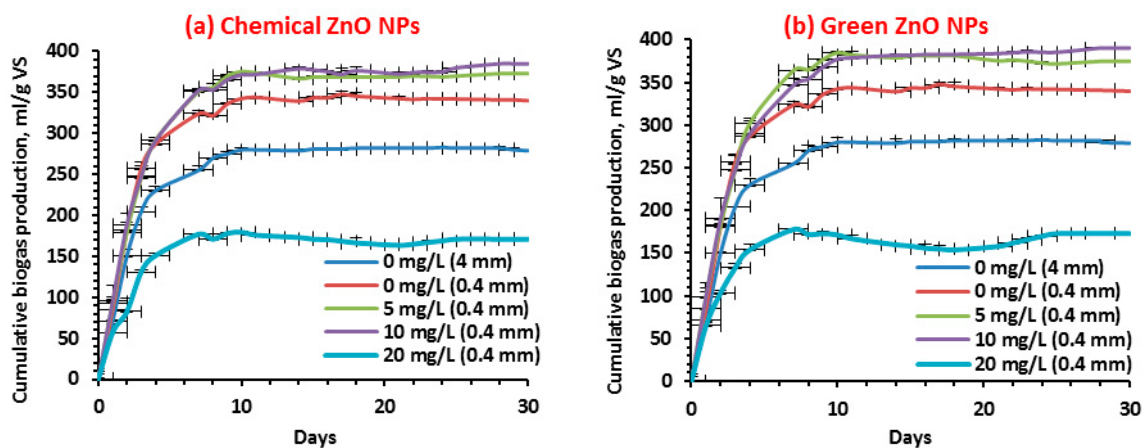

Figure 12. The mean cumulative net biogas production using (**a**) chemical and (**b**) green synthesized ZnO NPs.

The startup of mean biogas production yield is slightly enhanced when the mechanically treated barley straw is treated with 5 and 10 mg/L ZnO NPs compared with the biogas production yield without using both chemical and green synthesized ZnO NPs, as shown in Figure 12. The low doses of both chemical and green synthesized ZnO NPs (5 mg/L) have a significantly positive impact on biogas production ($p < 0.05$). Using 10 mg/L ZnO NPs produces higher biogas yield than 5 mg/L. It is also clear to notice that ZnO NPs concentration of 20 mg/L of both chemical and green synthesized ZnO NPs has negative effects on the biogas production. The biogas tests end when the daily production is less than 1% of the overall production for most of the operated tests, as noticed in Figure 13. On the other hand, it is clear to see that the mechanically treated barley straw of size 0.4 mm yields a biogas production of about 340 mL/g VS, which is higher than that of the untreated barley straw of size 4 mm, which yields about 279 mL/g VS.
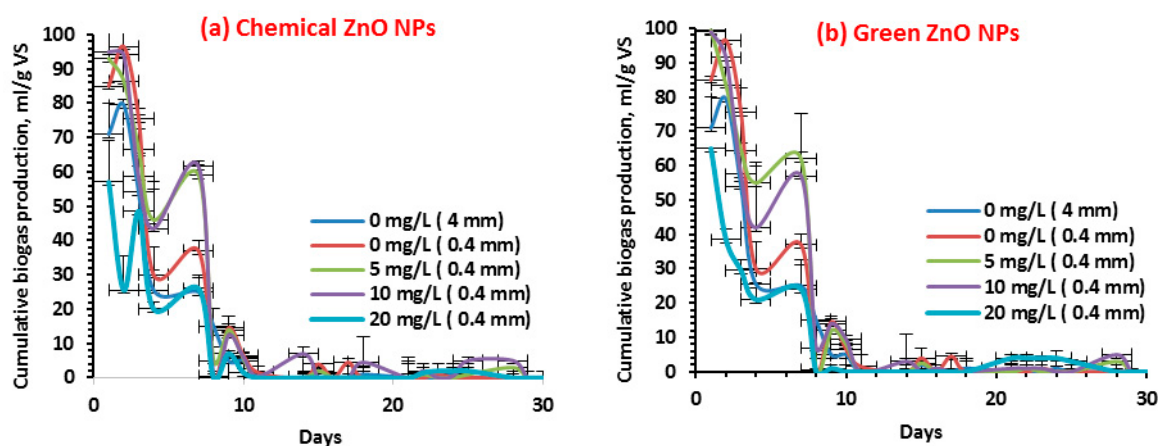
Figure 13. Mean rate percentage of daily biogas production using (**a**) chemical and (**b**) green synthesized ZnO NPs.

Mechanical pretreatment is the first step in splitting the constituents of lignocellulose, which are cellulose, lignin, hemicellulose, and other extracted components, and are related to the hydrogen bonds that bind the cellulose chain strongly in crystal form, which hinders the degradation of cellulose to glucose [5,14–16]. To solve the problems of biogas production based on lignocellulose and to enhance the efficiency of biogas production, it is essential to mechanically pretreat the substrates to increase feedstock utilization towards AD, which are to be fermented and NPs supplied with the substrate to enhance the enzymatic activity.

Besides, this study is the first study that examines the impact of mechanically treated barley straw in combination with the green synthesis of ZnO NPs on biogas production, which has resulted in a greater biogas yield in comparison with chemical ZnO NPs. The mechanical pretreatment enhances the surface area of reaction and biogas production, as confirmed by FTIR, XRD, SEM, and TGA. It is clear that mechanically pretreated barley straw (0.4 mm) has a good biogas yield, more than the untreated raw barley straw (4 mm) and with the same dosage of ZnO NPs due to the mechanical treatment, which increases the surface area of the reaction and enhances the AD, as shown in Figure 12. On the other hand, for 5 and 10 mg/L ZnO NPs, the mechanically pretreated barley straw has higher biogas yield due to the combined effect of both mechanical and chemical treatment.

Finally, for the 20 mg/L ZnO NPs, even if they are mechanically treated, the higher concentrations of ZnO NPs have inhibitory effects on the methanogenesis bacteria. From the above results, the order of biogas production can be arranged as mechanically and chemically treated barley straw with lower concentrations (5 and 10 mg/L) > mechanically treated barley straw 0.4 mm > raw untreated barley straw 4 mm > mechanically and chemically treated barley straw with higher concentrations (20 mg/L).
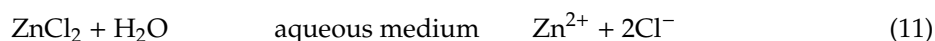
3.6. The Proposed Mechanism of ZnO NPs in Biogas Production

The specific effects of ZnO NPs on microorganisms in the AD system are hard to explain because the species of bacteria are not identified in the current study. In comparison, the exposure to ZnO NPs at various concentrations has different effects on the yield of biogas. ZnO NPs cause biogas inhibition at a large concentration (20 mg/L), about 50% for both green and chemical ZnO NPs, and the severity of the effect is directly related to the exposed concentration, which agrees with the reported data [63,64]. At a tolerable exposure of low concentrations of green (ZnO at 5 and 10 mg/L), there is a slight increase in the biogas production of about 10.3 and 14.9% and about 9.7 and 13.2% of chemical (ZnO at 5 and 10 mg/L), which agrees with the reported data [21,61], which have similar results with durum wheat.

When NPs are applied to the digester, the bacterial toxicity of NPs is reduced. This might have been due to agglomeration and adsorption into biomass, and this might be the reason for low toxicity in small concentrations of ZnO NPs, but this needs to be studied in depth for a clearer understanding, as previously mentioned [64]. ZnO NPs are actually dispersed in the solvent, not dissolved, and

therefore, they cannot release Zn^{2+} ions [64,65]. This may also explain why in our work, the low concentrations of ZnO NPs (5, 10 mg/L) do not release enough amount of Zn^{2+} ions that could inhibit bacterial activity. Moreover, the enhancement of biogas yield is due to the stress of anaerobic bacteria by introducing low dosages ZnO NPs, which enhance its resistance and may affect the bacterial activities, resulting in this slight increase in the biogas yield than control (mechanically treated barley straw with 0 mg/L ZnO NPs), but this also still needs further studies. These explanations may agree with previous work [66], who has studied the aerobic denitrifying bacteria and mentioned that to prevent ZnO NPs entering cells by adsorption, the production of extracellular polymeric substances (EPS) of two studied strains is increased by 13.2% and 43.9%, respectively. The up-regulation of amino sugar and carbohydrate-related metabolism has contributed to the increase of EPS production, and the increased nitrogen metabolism has contributed to higher activities of nitrate and nitrite reductases. The same study should be done in the future for anaerobic bacteria to study its metabolism pathways.

However, adding ZnO NPs 20 mg/L has made negative impacts on the biogas yield. This could be explained by a large amount of toxic Zn^{2+} ions, which are released from ZnO NPs that may damage the cell membrane of anaerobic bacteria, and then the anaerobic bacterial activity is reduced, even causing some anaerobic microbial death [65]. In our work, the amount of Zn^{2+} ions released by a high dose of ZnO NPs 20 mg/L is sufficient to reduce biogas yield by half, inhibiting the anaerobic bacteria. Since ZnO is amphoteric, it reacts with acids as well as alkalis, giving Zn^{2+} ions as in Equations (9)–(11) [64].

$$ZnO + HCl \qquad \text{acidic medium} \qquad ZnCl_2 + H_2O \tag{9}$$

$$ZnO + 2NaOH \qquad \text{acidic medium} \qquad Na_2ZnO_2 + H_2O \tag{10}$$

$$ZnCl_2 + H_2O \qquad \text{aqueous medium} \qquad Zn^{2+} + 2Cl^- \tag{11}$$

The free Zn^{2+} ions are instantly bound to the biomolecules due to their positive charge and negative charge on the biomolecules [64] like proteins and carbohydrates, and they no longer serve any essential role in the bacteria, as in Equation (12). Zn^{2+} ions are not always 100% bioavailable and may change invariably with physiological, redox potential, and pH [64,67], which needs more future studies.

$$Zn^{2+} + \text{Biomolecule} \qquad \text{Zn-biomolecule complex} \tag{12}$$

Mu and Chen [20] found that the methane yield was reduced by 18.3 and 75.1% from the control in the presence of 30 and 150 mg ZnO NPs/g TS, respectively. A high part of the reduction was usually related to the release of Zn^{2+} from the ZnO NPs. The reduction due to the release of Zn^{2+} ions was 9.4 and 63.8% for the equivalent of 30 and 150 mg ZnO NPs/g TS dose compared to the control, respectively. This would indicate that at higher ZnO NPs doses, the reduction is mainly caused by the release of Zn^{2+} rather than the NPs [68].

Wang et al. [63] mentioned that lower concentrations (1.3 and 4.6 µg/mL) of Fe^{2+} were found to enhance the AD, whereas higher concentrations (3.3 and 9.8 µg/mL) of Ag+ and Mg2+ were found to reduce the AD. Comparing the AD of sludge induced by nano zerovalent iron (nZVI), Ag NPs, or MgO NPs with that induced by the corresponding amounts of Fe^{2+}, Ag^+, and Mg^{2+}, it was found that the released Fe^{2+}, Ag^+, and Mg^{2+} were primarily responsible for the enhancement and/or inhibition impacts of nZVI, Ag NPs, and MgO NPs [63]. The contact between NPs and the bacterial cell wall is enough to make toxicity [64]. If it is right, then higher quantities of metal NPs are essential so that the bacterial cells are totally enveloped and protected from its environment, leaving no chance for nutrition to be absorbed to continue the life process. This may explain why in our work, the higher concentrations of ZnO NPs cause inhibition for biogas yield and reduce it by 50%.

It has been observed that the growth inhibition of microbes increases with raising the concentration of NPs. The incubation duration is supposed to be increased; the inhibition of growth will increase without any major changes in the mechanism of action [64,69]. For most experiments, the metal ions emitted from NPs play a significant role in the biological processes of microorganism populations.

Some scientists found that during the sewage sludge treatment process, higher metal ion dosages released from NPs have prevented these microorganisms from working [63].

Ganzoury et al. [70] specified that the higher surface area of NPs has a positive impact on the AD course. In this study, the higher biogas yield from green ZnO NPs than chemical one may be due to its higher surface area, as presented in Table 4. Other literature works [21,71] have shown that the green synthesized NPs are more stable and less toxic than chemical NPs, and this is one of the reasons to choose the extract of *A. plumula* in our study.

3.7. Kinetic Study

Tables 6 and 7 summarize the results of a kinetic study. The first-order, modified Gompertz, and logistic function models are found to have a good fit within the experimental data. In the experiment, mechanically treated barley straw (0.4 mm) with ZnO NPs concentration 20 mg/L exhibits the highest hydrolysis rates (K) of 0.537 d^{-1} (based on the first-order model) and 0.478 d^{-1} (based on the cone model). The maximum biogas production rate (Rm) of 1.60 L/g VS and 2.31 L/g VS is observed for the modified Gompertz model and the logistic function model, respectively. The late response and the subsequent adaptation of microorganisms to the fluctuating environment are expressed by the lag phase (λ) [37,72]. The modified Gompertz and the logistic function models have attained λ value of 0.9 days and 1.25 days, respectively. The value of λ, in this study, is relatively close to the previously reported λ of 1.2–1.8 days and 1.5–2.1 days (by Deepanraj et al. [73]) for the modified Gompertz model and logistic function model, respectively.

Table 6. Results of the kinetic study using the first order and cone models.

First-Order Kinetic Model					
Chemical					
Samples	**R^2**	**Predicted P (mL/g VS)**	**Differences%**	**K (1/day)**	**RMSE**
(4 mm)	0.995	282.03	1.1	0.387	5.5
(0.4 mm)	0.992	343.78	1.1	0.399	8.3
5 mg/L	0.995	373.50	0.1	0.356	7.2
10 mg/L	0.997	379.37	1.5	0.347	5.4
20 mg/L	0.977	172.08	0.6	0.44	6.9
Green					
5 mg/L	0.993	380.93	1.6	0.362	8.3
10 mg/L	0.999	386.53	1.1	0.334	3.9
20 mg/L	0.967	166.72	3.6	0.537	7.6
Cone Model					
Chemical					
Samples	**R^2**	**Predicted P (mL/g VS)**	**Differences%**	**K (1/day)**	**RMSE**
(4 mm)	0.760	275.96	1.1	0.329	21.62
(0.4 mm)	0.754	336.15	1.1	0.344	27.3
5 mg/L	0.758	363.90	2.4	0.316	30.83
10 mg/L	0.764	370.41	3.8	0.299	29.81
20 mg/L	0.745	168.01	1.7	0.4	13.86
Green					
5 mg/L	0.757	371.05	1.1	0.324	31.4
10 mg/L	0.769	377.73	12.6	0.283	29.4
20 mg/L	0.742	163.49	5.5	0.478	11.9

Table 7. Results of the kinetic study using the modified Gompertz and logistic function models.

Samples	R^2	Predicted P (mL/gVS)	Differences%	Rmax mL/g VS.day	λ (day)	RMSE
Modified Gompertz Model						
Chemical						
(4 mm)	0.991	279.03	0.01	1.46	0.736	6.24
(0.4 mm)	0.994	340.28	0.08	1.45	0.785	5.77
5 mg/L	0.995	369.73	0.87	1.60	0.651	4.58
10 mg/L	0.991	375.09	2.57	1.58	0.624	7.07
20 mg/L	0.982	171.24	0.14	1.37	0.777	5.30
Green						
5 mg/L	0.994	377.47	0.66	1.58	0.653	5.11
10 mg/L	0.988	381.93	2.20	1.60	0.852	8.23
20 mg/L	0.962	166.12	3.98	1.11	0.900	7.29
Logistic Function Model						
Chemical						
(4 mm)	0.981	278.16	0.30	2.05	0.736	9.3
(0.4 mm)	0.986	339.32	0.20	2.01	1.16	8.00
5 mg/L	0.987	368.57	1.19	2.27	0.952	7.29
10 mg/L	0.981	373.69	2.94	2.27	0.917	9.98
20 mg/L	0.978	170.96	0.021	1.97	1.12	5.08
Green						
5 mg/L	0.987	376.40	0.37	2.26	0.951	7.05
10 mg/L	0.976	380.14	2.65	2.31	0.863	11.52
20 mg/L	0.953	165.89	4.11	1.63	1.25	7.55

To evaluate the soundness of the model results in the four studied models, the predicted values for biogas production are plotted against the measured values, as presented in Figure 14. The low values—(3.9), (4.5), and (5.08)—of RMSE reflect the first order, modified Gompertz, and logistic function models and have a high ability to accurately predict the bioactivities, as opposed to the cone model (31.4). The statistical indicators (R^2) are given in Tables 6 and 7 to provide a picture of the kinetics study. Nguyen et al. [34] described that the higher value of R^2 (0.999, 0.995, and 0.987) and the lower values of RMSE for the first order, modified Gompertz, and logistic function models, respectively, indicated a more suitable kinetic model.
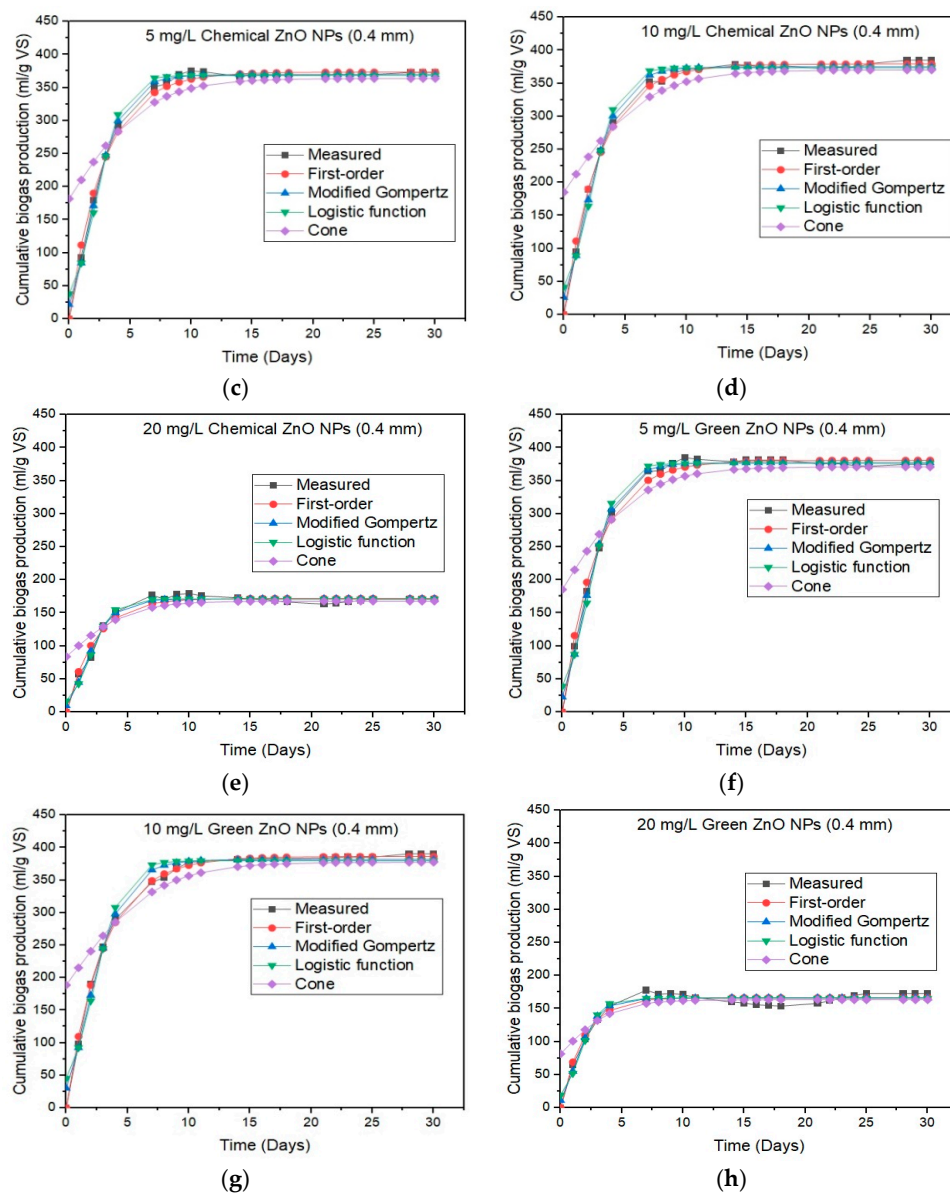

(a)

(b)
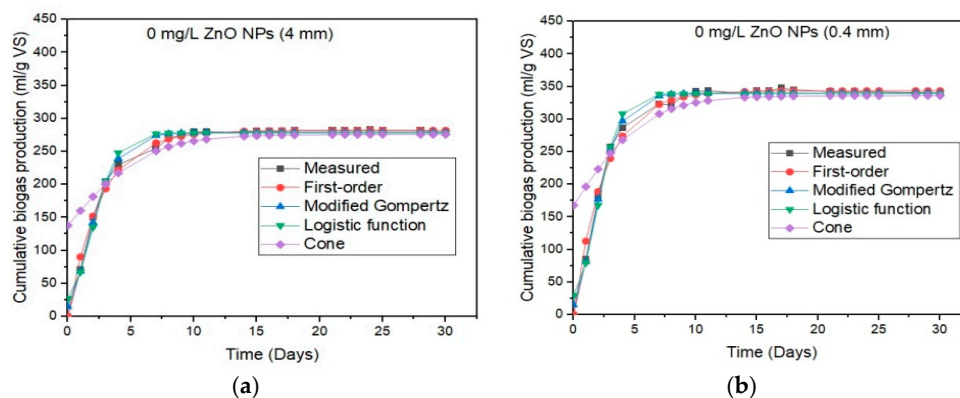
Figure 14. *Cont.*

Figure 14. Cumulative biogas yield from the four studied models. (**a**) 0 mg/L ZnO NPs (4 mm); (**b**) 0 mg/L ZnO NPs (0.4 mm); (**c**) 5 mg/L chemical ZnO NPs (0.4 mm); (**d**) 10 mg/L chemical ZnO NPs (0.4 mm); (**e**) 20 mg/L chemical ZnO NPs (0.4 mm); (**f**) 5 mg/L green ZnO NPs (0.4 mm); (**g**) 10 mg/L green ZnO NPs (0.4 mm); (**h**) 20 mg/L green ZnO NPs (0.4 mm).

3.8. The Cost-Benefit Analysis

The data for cost-benefit analysis, such as TS and VS, are taken from the biogas experiment whenever possible. Where the extra data are needed, such as field preparation and harvesting, they have been sourced from the relevant literature and personal communications, as shown in Scheme 1. Tables 8 and 9 show that the use of barley straw for biogas production is a practical option, and the biogas yield is comparable to previous studies [16]. However, it may be not profitable if barley straw is used instead of the current energy crops being used, such as wheat or maize.

Table 8. Cost-benefit for barley straw with and without mechanical pretreatment.

Cost	Units	Barley (4 mm)	Barley (0.4 mm)
Mechanical Treatment Cost for Barley Straw (chipping + milling)	€/ton	0	13.72
Chemicals (NPs + NaOH)	€/100g	0	0
Total	€/ha	871.11	884.83
Benefits			
Electricity Production (40% eff)	KWh/ha	969	1181
Electricity Sales	€/ha	62	76
Total	€/ha	62	76
Net Benefits	€/ha	−809.11	−808.83

Table 9. Cost-benefit for barley straw with combined mechanical and chemical pretreatment.

Cost	Units	5mg/L (0.4 mm)	10 mg/L (0.4 mm)	20 mg/L (0.4 mm)
Mechanical Treatment Price Needed for Barley Straw (chipping + milling)	€/ton	13.72	13.72	13.72
Chemicals (NPs + NaOH)	€/100g	5.52	5.52	5.52
Total	€/ha	890.35	890.35	890.35
Benefits				
Electricity Production (40% eff)	KWh/ha	1302	1356	601
Electricity Sales	€/ha	83	87	38
Total	€/ha	83	87	38
Net Benefits	€/ha	−807.35	−803.35	−852.35

From the results of the cost-benefit analysis shown in Tables 8 and 9, it is observed that with current costs and revenues, it is not profitable to use barley straw for biogas production. The significant differences in cumulative biogas production between the treated and untreated barley straw lead to higher specific methane yield. These differences translate to higher electricity production and higher revenues through electricity sales. Solely from the point of view of the revenues generated, the mechanically and chemically treated barley straw 10 mg/L (0.4 mm) gives the highest economic value. The net benefit of this cost-benefit analysis shows that the mechanically and chemically treated barely straw 10 mg/L (0.4 mm) is closest to profitability than the mechanically and chemically treated barely straw 5 mg/L (0.4 mm).

It is clear that to generate a profit in the future, it's a must to minimize costs. The cost of field preparation, crop cultivation, and fertilizer and pesticide application equals 542.35 €/ha, and to save this cost, the use of other crops, such as perennial crops that do not compete with the food chain and aquatic plants, appears to be the best option. Along with minimizing costs, there are some options to increase biogas production and associated revenue, such as digester type, co-digestion, and pretreatment method, which are considered the major factors that influence biogas production.

3.9. Levelized Cost of Energy

The LCOE depends on the biomass processing and treatment techniques, such as field preparation, crop cultivation, fertilizer and pesticide application, and mechanical and chemical treatment. The investment costs used to calculate LCOE and NPV are shown in Table 1. Figure 15 represents the LCOE of the untreated and treated barely straw. From Figure 15, it's clear to see that the combined mechanical and chemical treatment with 10 mg/L ZnO dosage can produce higher energy output. The LCOE decreases as the energy output (NPV) increases, as noticed in Figure 15. Specifically, the LCOE is computed based on the net present value of all costs (NPV) divided by the total amount of

energy produced over the energy system's lifetime [73]. The lowest value of LCOE is obtained for mechanically and chemically treated barley straw (0.4 mm + 10 mg/L ZnO), and the highest value is obtained for mechanically and chemically treated barley straw (0.4 mm + 20 mg/L ZnO).
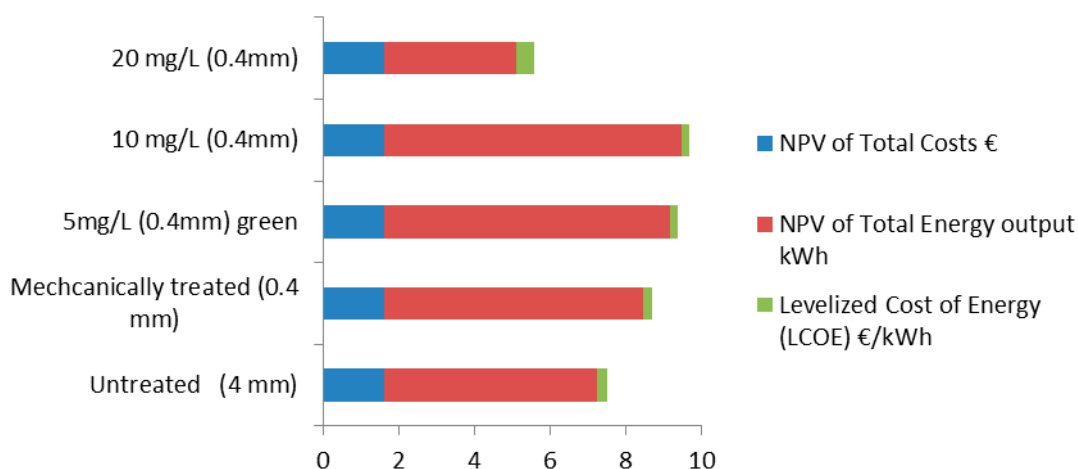

Figure 15. The net present value (NPV) € and levelized cost of energy (LCOE) €/kWh of the treated and untreated barley.

The average LCOE for the best mechanical and chemical treatments is 0.21 €/kWh, which can be considered non-competitive with the other candidate renewable energy systems, such as wind energy 0.068 €/kWh [74,75]. Moreover, the LCOE from biomass energy in this study is 200% higher than the LCOE from the biomass energy in Europe (0.088 €/kWh) in 2019 [76]. The reason for this high LCOE, as mentioned before, could be eliminated by choosing another aquatic crop with a high yield of biogas and choosing the suitable treatment techniques. Besides, changing the type of NPs, for example, iron oxide NPs, might have a good impact on the treatment processes and can be a good practical solution, as mentioned [63].

4. Conclusions

From the aforementioned results, it can be concluded that the mechanical pretreatment methods have improved the biodegradation of barley substrates and contributed to biogas enhancement with biogas yield 340 mL/g VS without adding ZnO NPs. There is a successful synthesis of green synthesized ZnO NPs using *A. plumula* extract, which contains phytochemicals components, acting as capping and stabilizing agents. Both morphology and the size of the synthesized ZnO NPs have been confirmed by SEM, FTIR, TEM, and EDX. The use of ZnO NPs in biogas is dosage-dependent, where the improvement of the biogas production is attained by adding 5 and 10 mg/L of ZnO NPs for mechanically treated barley straw. In particular, the biogas production yield is increased from 340 mL/g VS, using the barley biomass without ZnO NPs, to 385 and 390.5 mL/g VS, using 10 mg/L of chemical and green synthesized ZnO NPs, respectively. The green synthesized ZnO NPs provide a slightly higher biogas production yield than chemical synthesized ZnO NPs by 1 and 2% for 5 and 10 mg/L, respectively. The improvement of biogas production is about 14.9 and 13.2% for 10 mg/L of chemical and green synthesized ZnO NPs, respectively, more than mechanically treated barley straw of size 0.4 mm. But this improvement is still far from other NPs, such as nano zerovalent iron (nZVI) and Fe_2O_3 NPs with concentrations of 10 and 100 mg/g TSS, yielding more cumulative methane production levels at 120 and 117%, respectively, of the total biogas yield [63]. The mechanically treated barley straw of size 0.4 mm yields a higher biogas production of about 340 mL/g VS than the untreated barley straw of size 4 mm, which yields about 279 mL/g VS. Among the four kinetic models, the first-order model ($R^2 = 0.999$), modified Gompertz model ($R^2 = 0.995$), and logistic function model ($R^2 = 0.987$) are the most suitable models for fitting the measured biogas yield, and they could be used to describe the

kinetics of the AD process more reasonably. Based on the obtained results, the mechanically treated barley straw is a suitable source of biomass for biogas production, and the yields are higher than the untreated barley straw, but the cost-benefit analysis and LCOE show that it is not currently profitable to use barley straw for biogas production due to higher annual total cost. As a future development, the environmental analysis of the life cycle assessment (LCA) type could be also needed to evaluate the eco-compatibility of the bioprocess from barley straw in its entirety.

Author Contributions: Methodology, M.A.H. and A.P.; Software, M.A.H., A.P., F.S., and M.R.E.; Project administration, G.D.M.; Supervision, A.P. and A.E.N.; Writing—original draft, M.A.H., A.P., and M.R.E.; Writing—review and editing, M.A.H., A.P., M.R.E., A.E.N., S.R., A.E.S., and F.S. All authors have read and agreed to the published version of the manuscript.

Conflicts of Interest: The authors declare no conflict of interest.

Abbreviations

AD	Anaerobic digestion
NPs	Nanoparticles
ZnO NPs	Zinc oxide nanoparticles
LCOE	Levelized cost of energy
NPV	Net present value
GC/MS	Gas chromatography mass spectrometry
FTIR	Fourier transform infrared
FW	Full width
XRD	X-ray diffractograms
SEM	Scanning electron microscope
TEM	Transmission electron microscope
EDX	Energy-dispersive X-ray spectroscopy
BET	Brunauer–Emmett–Teller
TGA	Thermogravimetric analysis
TS	Total solids
Rm	The maximum biogas production rate (L/g VS added)
VS	Volatile solids
λ	The lag phase time (days)

References

1. Carlini, M.; Mosconi, E.M.; Castellucci, S.; Villarini, M.; Colantoni, A. An economical evaluation of anaerobic digestion plants fed with organic agro-industrial waste. *Energies* **2017**, *10*, 1165. [CrossRef]
2. Council of the European Union. *Directive of the European Parliament and of the Council on the Promotion of the Use of Energy from Renewable Sources*; Council of the European Union: Brussels, Belgium, 2018.
3. Tsavkelova, E.A.; Netrusov, A.I. Biogas production from cellulose containing substrates: A review. *Appl. Biochem. Microbiol.* **2012**, *48*, 421–433. [CrossRef]
4. Appels, L.; Lauwers, J.; Degrève, J.; Helsen, L.; Lievens, B.; Willems, K.; van Impe, J.; Dewil, R. Anaerobic digestion in global bio-energy production: Potential and research challenges. *Renew. Sustain. Energy Rev.* **2011**, *15*, 4295–4301. [CrossRef]
5. Feng, L.; Perschke, Y.M.L.; Fontaine, D.; Ward, A.J.; Eriksen, J.; Sorensen, P.; Moller, H.B. Co-ensiling of cover crops and barley straw for biogas production. *Renew. Energy* **2019**, *142*, 677–683. [CrossRef]
6. Monlau, F.; Barakat, A.; Trably, E.; Dumas, C.; Steyer, J.P.; Carrere, C. Lignocellulosic materials into biohydrogen and biomethane: Impact of structural features and pretreatment. *Crit. Rev. Environ. Sci. Technol.* **2011**, *43*, 260–322. [CrossRef]
7. Guerrieri, A.S.; Anifantis, A.S.; Santoro, F.; Pascuzzi, S. Study of a Large Square Baler with Innovative Technological Systems that Optimize the Baling Effectiveness. *Agriculture* **2019**, *9*, 86. [CrossRef]
8. Taherzadeh, M.J.; Karimi, K. Pretreatment of lignocellulosic wastes to improve ethanol and biogas production: A review. *Int. J. Mol. Sci.* **2008**, *9*, 1621–1651. [CrossRef]

9. Sun, L.; Müller, B.; Schnürer, A. Biogas production from wheat straw: Community structure of cellulose-degrading bacteria. *Energy Sustain. Soc.* **2013**, *3*, 15. [CrossRef]

10. Antognoni, S.; Ragazzi, M.; Rada, E.C.; Plank, R.; Aichinger, P.; Kuprian, M.; Ebner, C. Potential Effects of Mechanical Pre-treatments on Methane Yield from Solid Waste Anaerobically Digested. *Int. J. Environ. Bioremed. Biodegrad.* **2013**, *1*, 20–25.

11. Jędrczak, A.; Królik, D. Influence of paper particle size on the efficiency of digestion process. *Environ. Prot. Eng.* **2007**, *33*, 145–155.

12. Carrere, H.; Antonopoulou, G.; Affes, R.; Passos, F.; Battimelli, A.; Lyberatos, G.; Ferrer, I. Review of feedstock pretreatment strategies for improved anaerobic digestion: From lab-scale research to full-scale application. *Bioresour. Technol.* **2015**, *199*, 386–397. [CrossRef]

13. Kratky, L.; Jirout, T. Biomass size reduction machines for enhancing biogas production. *Chem. Eng. Technol.* **2011**, *34*, 391–399. [CrossRef]

14. Tsapekos, P.; Kougias, P.G.; Angelidaki, I. Biogas production from ensiled meadow grass; effect of mechanical pretreatments and rapid determination of substrate biodegradability via physicochemical methods. *Bioresour. Technol.* **2015**, *182*, 329–335. [CrossRef]

15. Tsapekos, P.; Kougias, P.G.; Egelund, H.; Larsen, U.; Pedersen, J.; Trenel, P.; Angelidaki, I. Mechanical pretreatment at harvesting increases the bioenergy output from marginal land grasses. *Renew. Energy* **2017**, *111*, 914–921. [CrossRef]

16. Balsari, P.; Menardo, S.; Airoldi, G. Effect of physical and thermal pre-treatment on biogas yield of some agricultural by-products. In *Progress in Biogas II*; German Society for Sustainable Biogas and Bioenergy Utilisation: Stuttgart, Hohenheim, Germany, 2011.

17. Abdelsalam, E.; Samer, M.; Attia, Y.A.; AbdelHadi, M.A.; Hassan, H.E.; Badr, Y. Influence of zero valent iron nanoparticles and magnetic iron oxide nanoparticles on biogas and methane production from anaerobic digestion of manure. *Energy J.* **2017**, *120*, 842–853. [CrossRef]

18. Amirante, R.; Demastro, G.; Distaso, E.; Hassaan, M.A.; Mormando, A.; Pantaleo, A.M.; Tamburrano, P.; Tedone, L.; Clodoveo, M.L. Effects of ultrasound and green synthesis ZnO nanoparticles on biogas production from Olive Pomace. *Energy Proced.* **2018**, *148*, 940–947.

19. Mu, H.; Chen, Y.; Xiao, N. Effects of metal oxide nanoparticles (TiO_2, Al_2O_3, SiO_2 and ZnO) on waste activated sludge anaerobic digestion. *Bioresour. Technol.* **2011**, *102*, 10305–10311. [CrossRef]

20. Mu, H.; Chen, Y. Long-term effect of ZnO nanoparticles on waste activated sludge anaerobic digestion. *Water Res.* **2011**, *45*, 5612–5620. [CrossRef]

21. Hassaan, M.A.; Pantaleo, A.; Tedone, L.; Elkatory, M.R.; Ali, R.M.; Nemr, A.E.; Mastro, G.D. Enhancement of biogas production via green ZnO nanoparticles: Experimental results of selected herbaceous crops. *Chem. Eng. Commun.* **2019**, 1–14. [CrossRef]

22. Kalpana, V.N.; Devi Rajeswari, V. A review on green synthesis, biomedical applications, and toxicity studies of ZnO NPs. *Bioinorganic Chem. Appl.* **2018**, *2018*, 3569758. [CrossRef]

23. Tian, Y.; Yang, K.; Zheng, L.; Han, X.; Xu, Y.; Li, Y.; Li, S.; Xu, X.; Zhang, H.; Zhao, L. Modelling Biogas Production Kinetics of Various Heavy Metals Exposed Anaerobic Fermentation Process Using Sigmoidal Growth Functions. *Waste Biomass Valoriz.* **2020**, *11*, 4837–4848. [CrossRef]

24. Pantaleo, A.; Villarini, M.; Colantoni, A.; Carlini, M.; Santoro, F.; RajabiHamedani, S. Techno-Economic Modeling of Biomass Pellet Routes: Feasibility in Italy. *Energies* **2020**, *13*, 1636. [CrossRef]

25. RajabiHamedani, S.; Villarini, M.; Colantoni, A.; Carlini, M.; Cecchini, M.; Santoro, F.; Pantaleo, A. Environmental and Economic Analysis of an Anaerobic Co-Digestion Power Plant Integrated with a Compost Plant. *Energies* **2020**, *13*, 2724. [CrossRef]

26. Said, M.; El-Shimy, M.; Abdelraheem, M.A. Photovoltaics energy: Improved modeling and analysis of the levelized cost of energy (LCOE) and grid parity–Egypt case study. *Sustain. Energy Technol. Assess.* **2015**, *9*, 37–48. [CrossRef]

27. American Public Health Association. *Standard Methods for the Examination of Water and Waste Water*; American Public Health Association: Washington, DC, USA, 1998; p. 874.

28. Gelegenis, J.; Georgakakis, D.; Angelidaki, I.; Mavris, V. Optimization of biogas production by co-digesting whey with diluted poultry manure. *Renew. Energ.* **2007**, *32*, 2147–2160. [CrossRef]

29. Trine, L.H.; Jens, E.S.; Irini, A.; Emilia, M.C.J.; Hans, M.; Thomas, H.C. Method for determination of methane potentials of solid organic waste. *Waste Manag.* **2004**, *24*, 393–400.

30. Nielfa, A.; Cano, R.; FdzPolanco, M. Theoretical methane production generated by the co-digestion of organic fraction municipal solid waste and biological sludge. *Biotechnol. Rep.* **2015**, *1*, 14–21. [CrossRef] [PubMed]

31. Remigi, E.U.; Buckley, C.A. *Co-Digestion of High Strength/Toxic Organic Effluents in Anaerobic Digesters at Wastewater Treatment Works*; Water Research Commission: Pretoria, South Africa, 2016.

32. Bhuyan, T.; Mishra, K.; Khanuja, M.; Prasad, R.; Varma, A. Biosynthesis of zinc oxide nanoparticles from Azadirachta indica for antibacterial and photocatalytic applications. *Mater. Sci. Semicond. Process.* **2015**, *32*, 55–61. [CrossRef]

33. Hassan, S.S.M.; ElAzab, W.I.M.; Ali, H.R.; Mansour, M.S.M. Green synthesis and characterization of ZnO nanoparticles for photocatalytic degradation of anthracene. *Adv. Nat. Sci. Nanosci. Nanotechnol.* **2015**, *6*, 1–12. [CrossRef]

34. Nguyen, D.D.; Jeon, B.H.; Jeung, J.H.; Rene, E.R.; Banu, J.R.; Ravindran, B.; Vu, C.M.; Ngo, H.H.; Guo, W.; Chang, S.W. Thermophilic Anaerobic Digestion of Model Organic Wastes: Evaluation of Biomethane Production and Multiple Kinetic Models Analysis. *Bioresour. Technol.* **2019**, *280*, 269–276. [CrossRef]

35. Kafle, G.K.; Chen, L. Comparison on Batch Anaerobic Digestion of Five Different Livestock Manures and Prediction of Biochemical Methane Potential (BMP) Using Different Statistical Models. *Waste Manag.* **2016**, *48*, 492–502. [CrossRef]

36. Donoso-Bravo, A.; Pérez-Elvira, S.I.; Fdz-Polanco, F. Application of Simplified Models for Anaerobic Biodegradability Tests. Evaluation of Pre-Treatment Processes. *Chem. Eng. J.* **2010**, *160*, 607–614. [CrossRef]

37. Li, L.; He, Q.; Zhao, X.; Wu, D.; Wang, X.; Peng, X. Anaerobic Digestion of Food Waste: Correlation of Kinetic Parameters with Operational Conditions and Process Performance. *Biochem. Eng. J.* **2018**, *130*, 1–9. [CrossRef]

38. Mohammed, M.; Egyir, I.S.; Donkor, A.K.; Amoah, P.; Nyarko, S.; Boateng, K.K.; Ziwu, C. Feasibility study for biogas integration into waste treatment plants in Ghana. *Egypt. J. Pet.* **2017**, *26*, 695–703. [CrossRef]

39. Uellendahl, H.; Wang, G.; Møller, H.B.; Jørgensen, U.; Skiadas, I.V.; Gavala, H.N.; Ahring, B.K. Energy balance and cost-benefit analysis of biogas production from perennial energy crops pretreated by wet oxidation. *Water Sci. Technol.* **2008**, *58*, 1841–1847. [CrossRef]

40. Schneider, L.; Haverinen, J.; Jaakkola, M.; Lassi, U. Pretreatment and fractionation of lignocellulosic barley straw by mechanocatalysis. *Chem. Eng. J.* **2017**, *327*, 898–905. [CrossRef]

41. Xu, Z.; Wang, Q.; Jianga, Z.H.; Yang, X.; Ji, Y. Enzymatic hydrolysis of pretreated soybean straw. *Biomass Bioenergy* **2007**, *31*, 162–167. [CrossRef]

42. Karuppiah, T.; Azariah, V.E. Biomass pretreatment for enhancement of biogas production. In *Anaerobic Digestion*; IntechOpen: London, UK, 2019.

43. Sanchez-Silva, L.; López-González, D.; Villaseñor, J.; Sánchez, P.; Valverde, J.L. Thermogravimetric-mass spectrometric analysis of lignocellulosic and marine biomass pyrolysis. *Bioresour. Technol.* **2012**, *109*, 163–172. [CrossRef]

44. Carrier, M.; Loppinet-Serani, A.; Denux, D.; Lasnier, J.M.; Ham-Pichavant, F.; Cansell, F.; Aymonier, C. Thermogravimetric analysis as a new method to determine the lignocellulosic composition of biomass. *Biomass Bioenergy* **2011**, *35*, 298–307. [CrossRef]

45. Hassaan, M.; El Katory, M.; Ali, R.M.; El Nemr, A. Photocatalytic degradation of reactive black 5 using Photo-Fenton and ZnO nanoparticles under UV irradiation. *Egypt. J. Chem.* **2020**, *63*, 17–18. [CrossRef]

46. Soliman, E.A.; Elkatory, M.R.; Hashem, A.I.; Ibrahim, H.S. Synthesis and performance of maleic anhydride copolymers with alkyl linoleate or tetra-esters as pour point depressants for waxy crude oil. *Fuel* **2018**, *211*, 535–547. [CrossRef]

47. Ali, R.M.; Elkatory, M.R.; Hamad, H.A. Highly active and stable magnetically recyclable CuFe2O4 as a heterogenous catalyst for efficient conversion of waste frying oil to biodiesel. *Fuel* **2020**, *268*, 117297. [CrossRef]

48. Xu, C.X.; Sun, X.W.; Dong, Z.L.; Cui, Y.P.; Wang, B.P. Nanostructured singlecrystalline twin disks of zinc oxide. *Cryst. Growth Des.* **2007**, *7*, 541–544. [CrossRef]

49. Ashkenov, N.; Mbenkum, B.N.; Bundesmann, C.; Riede, V.; Lorenz, M.; Spemann, D.; Kaidashev, M.; Kasic, A.; Schubert, M.; Grundmann, M.; et al. Infrared dielectric functions and phonon modesof high-quality ZnO films. *J. Appl. Phys.* **2003**, *93*, 1. [CrossRef]

50. Alim, K.A.; Fonoberov, V.A.; Balandin, A.A. Origin of the optical phonon frequency shifts in ZnO quantum dots. *Appl. Phys. Lett.* **2005**, *86*, 05103. [CrossRef]

51. Sivakami, R.; Dhanuskodi, S.; Karvembu, R. Estimation of lattice strain in nanocrystalline RuO2 by Williamson–Hall and size–strain plot methods. *Spectrochim. Acta Part A Mol. Biomol. Spectrosc.* **2016**, *152*, 43. [CrossRef]

52. Ali, R.M.; Hassaan, M.A.; Elkatory, M.R. Towards Potential Removal of Malachite Green from Wastewater: Adsorption Process Optimization and Prediction. In *Materials Science Forum*; Trans Tech Publications Ltd.: Bäch, Suisse, 2020; p. 1008.

53. Ismail, M.A.; Taha, K.K.; Modwi, A.; Khezami, L. ZnO nanoparticles: Surface and X-ray profile analysis. *J. Ovonic Res.* **2018**, *14*, 381–393.

54. Khan, M.; Cao, W. Cationic (V, Y)-codoped TiO2 with enhanced visible light induced photocatalytic activity: A combined experimental and theoretical study. *J. Appl. Phys.* **2013**, *114*, 183514. [CrossRef]

55. Burton, A.W.; Ong, K.; Rea, T.; Chan, I.Y. On the estimation of average crystallite size of zeolites from the Scherrer equation: A critical evaluation of its application to zeolites with one-dimensional pore systems. *Microporous Mesoporous Mater.* **2009**, *117*, 75–90. [CrossRef]

56. Friis, J.; Holm, C.; Halling-Sørensen, B. Evaluation of elemental composition of algal biomass as toxical endpoint. *Chemosphere* **1998**, *13*, 2665–2676. [CrossRef]

57. Pang, Y.Z.; Liu, Y.P.; Li, X.J.; Wang, K.S.; Yuan, H.R. Improving biodegradability and biogas production of corn stover through sodium hydroxide solid state pretreatment. *Energy Fuels* **2008**, *22*, 2761–2766. [CrossRef]

58. Nyns, E.J. *Biomethanation Processes*; Wiley-VCH: Weinheim, Berlin, Germany, 1986; pp. 207–267.

59. Kivaisi, A.K.; Mtila, M. Production of biogas from water hyacinth (Eichhorniacrassipes) in a two stage bioreactor. *World J. Microbiol. Biotechnol.* **1997**, *14*, 125–131. [CrossRef]

60. Mshandete, A.; Kivaisi, A.; Rubindamayugi, M.; Mattiasson, B. Anaerobic batch co-digestion of sisal pulp and fish wastes. *Bioresour. Technol.* **2004**, *95*, 19–24. [CrossRef] [PubMed]

61. Hassaan, M.A.; Pantaleo, A.; Tedone, L.; Demastro, G. Biogas production from silage flour wheat influenced by chemical and green synthesized ZnO nanoparticles. In Proceedings of the XLVII Conference of Italian Society for Agronomy, Marsala, Italy, 12–14 September 2018.

62. Elijah, T.; Ibifuro, A.; Yahaya, S.M. The study of cow dung as co-substrate with rice husk in biogas production. *Sci. Res. Essay* **2009**, *9*, 861–866.

63. Wang, T.; Zhang, D.; Dai, L.; Chen, Y.; Dai, X. Effects of metal nanoparticles on methane production from waste-activated sludge and microorganism community shift in anaerobic granular sludge. *Sci. Rep.* **2016**, *6*, 1–10. [CrossRef]

64. Siddiqi, K.S.; Rahman, A.; Husen, A. Properties of zinc oxide nanoparticles and their activity against microbes. *Nanoscale Res. Lett.* **2018**, *13*, 1–13. [CrossRef]

65. Chen, Y.; Yang, Z.; Zhang, Y.; Xiang, Y.; Xu, R.; Jia, M.; Cao, J.; Xiong, W. Effects of different conductive nanomaterials on anaerobic digestion process and microbial community of sludge. *Bioresour. Technol.* **2020**, *304*, 123016. [CrossRef]

66. Ma, T.F.; Chen, Y.P.; Fang, F.; Yan, P.; Shen, Y.; Kang, J.; Nie, Y.D. Effects of ZnO nanoparticles on aerobic denitrifying bacteria Enterobacter cloacae strain HNR. *Sci. Total Environ.* **2020**, *725*, 138284. [CrossRef]

67. Lin, D.; Xing, B. Phytotoxicity of nanoparticles: Inhibition of seed germination and root growth. *Environ. Pollut.* **2007**, *150*, 243–250. [CrossRef]

68. Olaya, W.B. Effect of Size, Coating and Concentration of Zinc Oxide Nanoparticles on Anaerobic Digestion of Municipal Wastewater Sludge. Ph.D. Thesis, University of British Columbia, Vancouver, BC, Canada, 2019.

69. Brayner, R.; Ferrari-Iliou, R.; Brivois, N.; Djediat, S.; Benedetti, M.F.; Fiévet, F. Toxicological impact studies based on Escherichia coli bacteria in ultrafine ZnO nanoparticles colloidal medium. *Nano Lett.* **2006**, *6*, 866–870. [CrossRef]

70. Ganzoury, M.A.; Allam, N.K. Impact of nanotechnology on biogas production: A mini-review. *Renew. Sustain. Energy Rev.* **2015**, *50*, 1392–1404. [CrossRef]

71. Franklin, N.M.; Rogers, N.J.; Apte, S.C.; Batley, G.E.; Gadd, G.E.; Casey, P.S. Comparative toxicity of nanoparticulate ZnO, bulk ZnO, and ZnCl2 to a freshwater microalga (*Pseudokirchneriella subcapitata*): The importance of particle solubility. *Environ. Sci. Technol.* **2007**, *41*, 8484–8490. [CrossRef] [PubMed]

72. Deepanraj, B.; Sivasubramanian, V.; Jayaraj, S. Experimental and Kinetic Study on Anaerobic Digestion of FoodWaste: The E_ect of Total Solids and PH. *J. Renew. Sustain. Energy* **2015**, *7*, 063104. [CrossRef]

73. Mao, C.; Wang, X.; Xi, J.; Feng, Y.; Ren, G. Linkage of Kinetic Parameters with Process Parameters and Operational Conditions during Anaerobic Digestion. *Energy* **2017**, *135*, 352–360. [CrossRef]

74. Abdelhady, S.; Borello, D.; Shaban, A. Assessment of levelized cost of electricity of offshore wind energy in Egypt. *Wind Eng.* **2017**, *41*, 160–173. [CrossRef]

75. DLR. *German Aerospace Center Concentrating Solar Power for the Mediterranean Region (Report by order of Federal Ministry for the Environment)*; DLR: Berlin, Germany, 2005; Available online: www.dlr.de/tt/med-csp (accessed on 30 July 2020).

76. Hansen, K. Decision-making based on energy costs: Comparing levelized cost of energy and energy system costs. *Energy Strategy Rev.* **2019**, *24*, 68–82. [CrossRef]